Finite-range Coulomb gas models. II. Applications to quantum kicked rotors and banded random matrices

Avanish Kumar, Akhilesh Pandey, and Sanjay Puri
School of Physical Sciences, Jawaharlal Nehru University, New Delhi 110067, India

(Received 29 July 2019; revised manuscript received 3 January 2020; accepted 31 January 2020; published 24 February 2020)

In part I of this two-stage exposition [Pandey, Kumar, and Puri, preceding paper, Phys. Rev. E **101**, 022217 (2020)], we introduced finite-range Coulomb gas (FRCG) models, and developed an integral-equation framework for their study. We obtained exact analytical results for $d = 0, 1, 2$, where d denotes the range of eigenvalue interaction. We found that the integral-equation framework was not analytically tractable for higher values of d. In this paper, we develop a Monte Carlo (MC) technique to study FRCG models. Our MC simulations provide a solution of FRCG models for arbitrary d. We show that, as d increases, there is a transition from Poisson to Wigner-Dyson classical random matrix statistics. Thus FRCG models provide a route for transition from Poisson to Wigner-Dyson statistics. The analytical formulation obtained in part I, and MC techniques developed in this paper, are used to study banded random matrices (BRMs) and quantum kicked rotors (QKRs). We demonstrate that, for a BRM of bandwidth b and a QKR of chaos parameter α, the appropriate FRCG model has range $d = b^2/N = \alpha^2/N$, for $N \to \infty$. Here, N is the dimensionality of the matrix in the BRM, and the evolution operator matrix in the QKR.

DOI: 10.1103/PhysRevE.101.022218

I. INTRODUCTION

Random matrices [1–4] have found extensive applications in quantum chaos, i.e., the study of quantum systems the classical counterpart of which is chaotic [5–10]. The connection between quantum chaos and random matrices is well established [11,12]. An important paradigm of quantum chaotic systems is the quantum kicked rotor (QKR) [7,8,10]. The Hamiltonian of the QKR is periodic in time with a delta-function perturbation. In Ref. [13], we introduced and analytically studied finite-range Coulomb gas (FRCG) models which define classes of random matrix ensembles. These are parametrized by the range of eigenvalue interactions, denoted as d.

In this paper, we demonstrate the applicability of FRCG models to quantum chaotic systems. We show that spectral fluctuations of the time evolution operator over one period (i.e., the Floquet operator) of the QKR can be modeled by FRCG models. In other applications, FRCG models have also been used to study quantum pseudointegrable systems [14,15]. We expect that they would also be applicable to many other physical systems.

An unusual property of quantum chaos is the suppression of chaotic diffusion. In classically chaotic systems such as the classical kicked rotor, the average energy of the system grows linearly with time. However, in its quantum chaotic counterpart (i.e., the QKR), the average energy saturates in time. The suppression of diffusion in the QKR is also known as *dynamical localization* [16]. The origin of this phenomenon lies in the localization of wave functions of the Floquet operator in the momentum basis [17–20]. In this context, many studies have focused on the transition from ergodic (Wigner-Dyson statistics) to integrable behavior (Poisson statistics) in disordered systems [19–22]. The operator corresponding to the Hamiltonian of quantum systems exhibiting localization can be described by banded random matrices (BRMs). Therefore, the eigenvalue statistics of BRM ensembles can also be modeled by FRCG ensembles.

The organization of this paper is as follows. In Sec. II, we discuss the Monte Carlo (MC) technique for FRCG models. In Sec. III, we present MC results for FRCG, and compare with analytical results given in Secs. IV–VI of Ref. [13]. In Sec. IV, we define QKRs and BRMs and discuss their connection with FRCG models. We introduce an effective range d, which is determined by the parameters of the QKR. In Sec. V, we present a detailed comparison of FRCG results (analytical and MC) and numerical results for the QKR and BRM. In particular, we will focus on the crossover from Poison to classical ensemble statistics as d increases. In Sec. VI, we discuss FRCG models for fractional values of d, and present their applications in QKRs. In Sec. VII, we summarize the results presented in this paper.

It is appropriate to highlight the results here as compared to our earlier short paper on this subject [23]. Here, we present details of our MC techniques for the FRCG models. We provide MC results for FRCG models, showing the crossover from Poisson to Wigner-Dyson statistics as d increases. We present results for a wide range of spectral quantities of BRMs and QKRs (e.g., spacing distributions, spacing variance, correlation functions, etc.), and it is shown that both of these systems can be described very well by FRCG models. Finally,

we provide additional results for QKR and FRCG models with fractional values of d.

II. MONTE CARLO TECHNIQUE FOR FRCG MODELS

As mentioned in Ref. [13], it becomes harder to obtain complete analytical results for FRCG models with higher values of d. However, MC results are easily calculable for arbitrary d, thereby providing us a complete picture of FRCG models. In this section, we discuss the MC method. The MC results will supplement our earlier exact results in Ref. [13].

From Ref. [13], we recall the equilibrium joint probability density (JPD) for the linear case:

$$p(x_1, \ldots, x_N) = C \exp(-\beta W), \tag{1}$$

where the eigenvalues x_j are in ascending order. The potential W has a two-body logarithmic potential, and one-body confining potential

$$W = -{\sum}' \log|x_j - x_k| + \sum_j V(x_j). \tag{2}$$

Here, $\sum'$ denotes a sum over all $|j-k| \leqslant d$ with $j \neq k$, and d denotes the range of the interaction in terms of the particle indices.

The corresponding equilibrium JPD for the circular case is

$$p(\theta_1, \ldots, \theta_N) = C \exp(-\beta W), \tag{3}$$

where the eigenangles θ_j are arranged on a unit circle in ascending order. The potential W is given by

$$W = -\frac{1}{2}{\sum}' \log|e^{i\theta_j} - e^{i\theta_k}| + \sum_j V(\theta_j). \tag{4}$$

In this case, $V(\theta)$ is a potential periodic on the unit circle. Both the linear and the circular JPDs yield the well-known classical ensembles for $d = N-1$. We will shortly describe an MC method for sampling the above JPDs.

An equivalent formulation uses the Langevin equation [24]. In the linear case, the Langevin equation for eigenvalues $\{x_j\}$ is [25]

$$\frac{dx_j}{d\tau} = \beta E_j + w_j(\tau). \tag{5}$$

Here, E_j is the force arising from the potential in Eq. (2):

$$E_j = -\frac{\partial W}{\partial x_j}. \tag{6}$$

The w_j in Eq. (5) denotes a Gaussian white noise which obeys the appropriate fluctuation-dissipation relation. A similar Langevin equation is obtained for the circular case where $x_j \to \theta_j$. One can numerically solve these stochastic differential equations (with adequate precautions to avoid level crossing) to obtain the equilibrium spectra. The Langevin method is not as efficient as the MC method for obtaining equilibrium JPDs. However, if one is interested in nonequilibrium evolution also, the Langevin approach will be the method of choice. We will not focus on the Langevin approach in this paper.

Our MC approach follows Ref. [26] for the linear case of Eq. (1), and Ref. [27] for the circular case of Eq. (3).

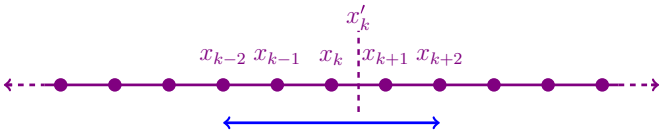

FIG. 1. Schematic of the MC technique to generate eigenvalue spectra for FRCG models. We consider the case of linear ensembles. The particles on the line denote the positions of the eigenvalues $\{x_j\}$. The eigenvalues interact up to a range $d = 2$ in the case shown. This range is measured in terms of the particle indices. In an attempted MC move, the particle x_k is displaced with uniform probability to x'_k in the range (x_{k-1}, x_{k+1}). The move is accepted with a probability $\exp(-\beta \triangle W)$, where ΔW is the change in the potential in Eq. (2). An MCS corresponds to N attempted moves. The independent spectra are realized by sampling the MC evolution at suitable intervals.

Because of the logarithmic singularity in the corresponding potentials, particle positions cannot change their order. Our MC implementation directly respects this constraint, resulting in a more efficient calculation of the equilibrium JPD (see Fig. 1).

In the *linear case*, we take a set of N eigenvalues $(x_1, \ldots, x_N)$ ordered sequentially on a real line with fixed boundaries. The boundaries are chosen such that the probability of finding an eigenvalue outside the range is negligible. A stochastic move assigns, to any randomly chosen x_k, the new position x'_k between (x_{k-1}, x_{k+1}) with a uniform probability. The move is accepted with a probability $\exp(-\beta \triangle W)$, where ΔW is the change in the potential in Eq. (2) after the stochastic move. A Monte Carlo step (MCS) corresponds to N attempted moves.

In the *circular case*, we take a set of N eigenvalues $(e^{i\theta_1}, e^{i\theta_2}, \ldots, e^{i\theta_N})$ ordered sequentially on the unit circle. A stochastic move assigns to a randomly chosen eigenangle θ_j the new position $\theta'_j \in (\theta_{j-1}, \theta_{j+1})$ with a uniform probability. After each eigenangle movement, we use periodic boundary conditions: θ'_j is computed modulo 2π. (This respects the original order of their positions on a circle). The move is accepted with a probability $\exp(-\beta \triangle W)$, where ΔW is the change in the potential in Eq. (4) after the stochastic move.

In Sec. III, we compare MC and analytical results (from Ref. [13]) for the level density and fluctuation measures. We will demonstrate that MC results are in excellent agreement with the analytical results, whenever these are available. Our purpose is to establish the MC technique as a method of obtaining "exact results" for higher values of d, where analytical results are not available.

All MC results for spectral properties presented in this paper are obtained as averages over 1000 independent spectra of dimension $N = 1001$. For fluctuation measures, we will show results for all three β values and the Poisson case ($\beta = 0$).

III. MONTE CARLO RESULTS FOR LEVEL DENSITY AND FLUCTUATION MEASURES

In this section, we present MC results for the level density in linear ensembles. In the uniform circular case, the level density is constant. We also present MC results for the fluctua-

tion measures for many d values, which confirm the transition from Poisson ($d = 0$) to classical ($d = N - 1$) ensembles.

In Ref. [13], we have presented analytical results for the level density in the linear ensembles with an arbitrary potential. Here, we compare the MC results for the level density with the corresponding exact results for the quartic potential. We have studied this potential for $d = O(1)$ and $O(N)$. In each case, excellent agreement is found. Let us show some representative results. We consider the linear case with the quartic potential:

$$V(x) = \kappa\left(\frac{x^4}{4} - \alpha\frac{x^2}{2}\right), \quad \kappa > 0. \tag{7}$$

Here, κ sets the scale of the V axis. In the quartic potential, α determines whether the potential is single well ($\alpha < 0$) or double well ($\alpha > 0$). For $d = N - 1$, there is a critical value α_c such that the level density makes a transition from a one-band density ($\alpha < \alpha_c$) to a two-band density ($\alpha > \alpha_c$) [26]. For $d = O(1)$, the density is given in Eq. (29) of Ref. [13]. This is shown in Fig. 2 for $d = 2$. For $d = O(N)$, the density is given in Eqs. (46) and (47) of Ref. [13] (see Fig. 3). Figures 2 and 3 demonstrate that the level density obtained by the MC technique is numerically indistinguishable from the corresponding analytical results. We have confirmed (not shown here) that the same applies for fluctuation measures for FRCG models with $d = 1, 2$. Therefore, we will subsequently equate MC results with exact results for FRCG models with arbitrary d.

Next we present some results for fluctuation measures for different d values. Figure 4 corresponds to the nearest-neighbor spacing distribution for $d = 0, 1, 2, 5, 10$ and $\beta = 1, 2, 4$. For comparison, the respective classical results have also been plotted. We can see that the MC data for $d = 10$ are already very close to the classical result. In Fig. 5, we plot the two-point correlation functions [$R_2(s)$ vs s] for $d = 0, 1, 2, 3, 5$ for all three β values. Figure 6 shows the two-point cluster function, which is defined as $Y_2(s) = 1 - R_2(s)$. In Fig. 7, we show the number variance [$\Sigma^2(r)$ vs r] for $d = 0, 1, 2, 5, 10, 25$ and $\beta = 1, 2, 4$. For comparison, we have also plotted the classical random matrix theory (RMT) results. The transition from Poisson to Gaussian ensembles as d is increased from zero to $N - 1$ is very clear.

Before concluding this section, it is useful to compare our MC results with the mean-field (MF) results discussed in Sec. IX of Ref. [13]. In Fig. 8, we plot the spacing density [$p_{n-1}(s)$ vs s] for various values of n, d, and β. The MF result for $p_{n-1}(s)$ is given in Eq. (91) of Ref. [13]. In all cases shown, we find very good agreement between MF results and the exact MC results.

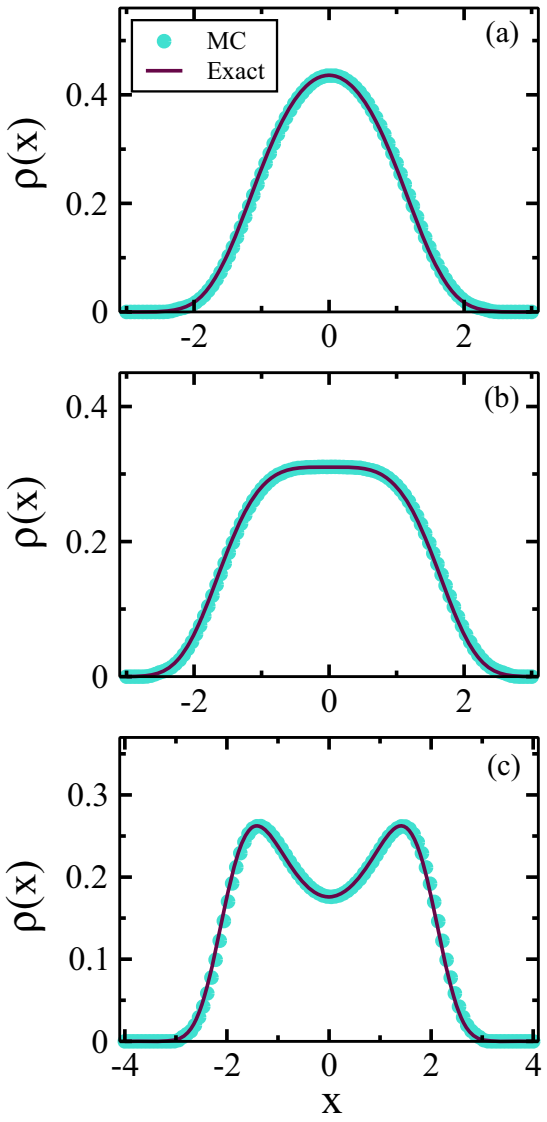

FIG. 2. Level density for the $d = 2$ FRCG model with $\beta = 2$. We used the quartic potential with $\kappa = 1$, and (a) $\alpha = -2$, (b) $\alpha = 0$, and (c) $\alpha = 2$. The filled circles correspond to MC results, and the solid lines are analytical results from Eq. (29) in Ref. [13].

IV. PHYSICAL APPLICATIONS OF FRCG MODELS

Let us now demonstrate the applicability of the FRCG models to two important physical applications, i.e., the QKR and BRM. The QKR is a prototypical example of quantum chaotic systems. The spectral fluctuations of QKR in the strongly chaotic regime correspond to the classical random matrix or Wigner-Dyson statistics [28,29]. This statistics can be obtained from infinite-range Coulomb gas models, as discussed in Sec. II of Ref. [13] (see also Ref. [30]). In the following sections, we demonstrate that spectral fluctuations of QKRs are described by FRCG models. Earlier work has also shown a deep connection between QKRs and BRMs [16,17]. Therefore, the statistics of BRM ensembles is also described by FRCG models. In this section, we introduce QKRs and BRMs and give their definitions.

A. Quantum kicked rotors

Following Izrailev [28], we consider a finite-dimensional [$N \times N$] matrix model for QKRs. The evolution operator is given by $U = BG$, where

$$B(\alpha) = \exp\left[-i\frac{\alpha}{\hbar}\cos(\theta + \theta_0)\right], \tag{8}$$

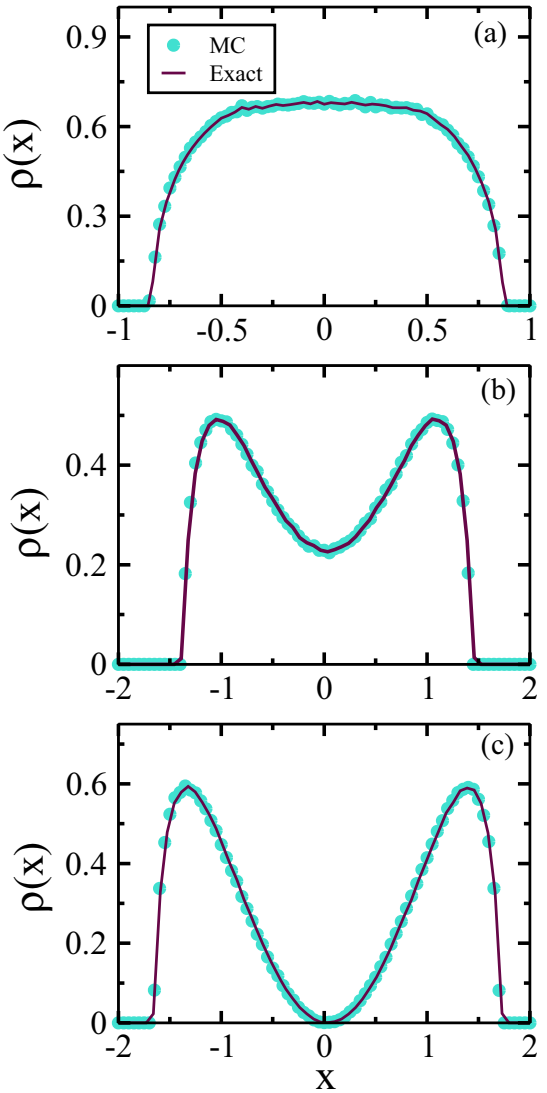

FIG. 3. Level density for the $d = 750$ FRCG model with $\beta = 2$. We used the quartic potential with $\kappa = 1$, and (a) $\alpha = -2$, (b) $\alpha = 0$, and (c) $\alpha = \alpha_c = 1.414$. The filled circles correspond to MC results, and the solid lines are analytical results from Eqs. (46) and (47) in Ref. [13].

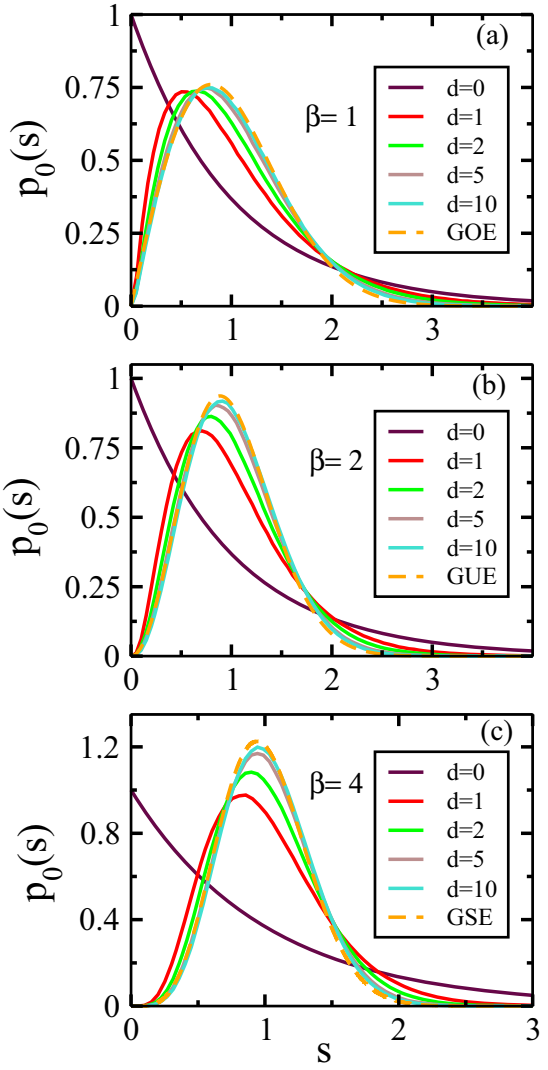

FIG. 4. Comparison of nearest-neighbor spacing distribution [$p_0(s)$ vs s] for FRCG models with $d = 0, 1, 2, 5, 10$. We show results for (a) $\beta = 1$, (b) $\beta = 2$, and (c) $\beta = 4$. In each frame, the dashed line denotes the classical Gaussian ensemble result.

and

$$G = \exp\left[-\frac{i}{2\hbar}(p+\gamma)^2\right], \tag{9}$$

with θ and p being the position and momentum operators. Here, α is the kicking parameter, θ_0 is the parity-breaking parameter, and γ is the time-reversal-breaking parameter ($0 \leqslant \gamma < 1$). In position representation,

$$B_{mn} = \exp\left[-i\frac{\alpha}{\hbar}\cos\left(\frac{2\pi m}{N}+\theta_0\right)\right]\delta_{mn}, \tag{10}$$

$$G_{mn} = \frac{1}{N}\sum_{l=-N'}^{N'} \exp\left[-i\left(\frac{\hbar}{2}l^2 - \gamma l - \frac{2\pi\mu l}{N}\right)\right], \tag{11}$$

where $N' = (N-1)/2$. The indices $m, n = -N', -N'+1, \ldots, N'$. Then, the evolution operator becomes

$$U_{mn} = \frac{1}{N}\exp\left[-i\alpha\cos\left(\frac{2\pi m}{N}+\theta_0\right)\right] \times \sum_{l=-N'}^{N'} \exp\left[-i\left(\frac{l^2}{2} - \gamma l - \frac{2\pi\mu l}{N}\right)\right], \tag{12}$$

where $\mu = m - n$. We have set $\hbar = 1$. One knows that, when parity is broken ($\theta_0 \neq 0$), and $\alpha^2 \gg N \gg 1$, then the eigenvalue spectra of U accurately exhibit classical random matrix spectral fluctuations (e.g., spacing distribution and number variance). For $\gamma = 0$, the fluctuations are characterized by $\beta = 1$ [Gaussian orthogonal ensemble (GOE)]. For $\gamma \neq 0$ ($\gamma \gg N^{-3/2}$), the fluctuations obey $\beta = 2$ [Gaussian unitary ensemble (GUE)] statistics [28,31].

The numerical results presented in this paper for the spectral statistics of QKRs were obtained by studies of the matrix

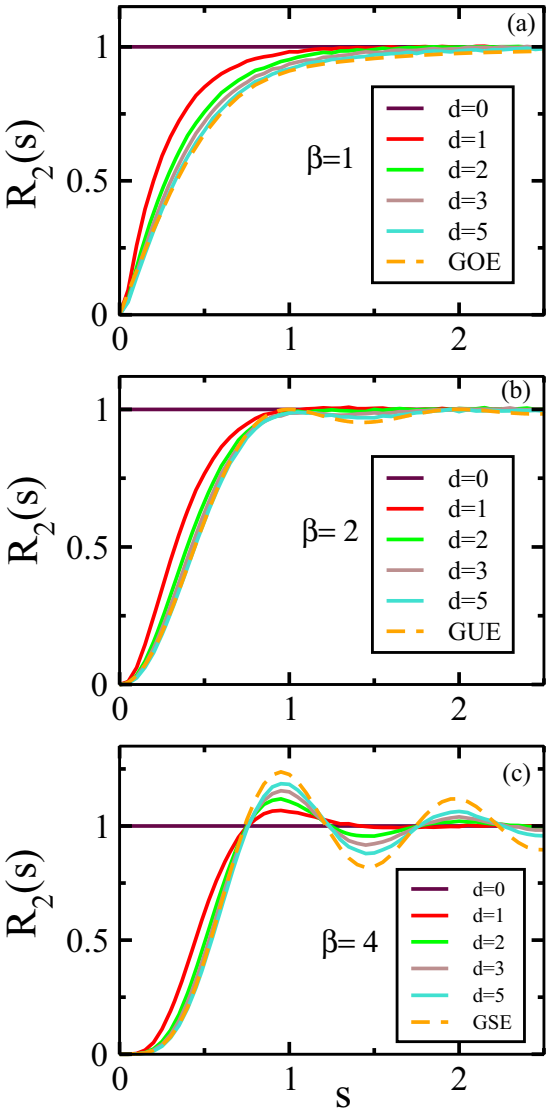

FIG. 5. Comparison of the two-point correlation function [$R_2(s)$ vs s] for FRCG models with $d = 0, 1, 2, 3, 5$. We show results for (a) $\beta = 1$, (b) $\beta = 2$, and (c) $\beta = 4$. In each frame, the dashed line denotes the classical Gaussian ensemble result.

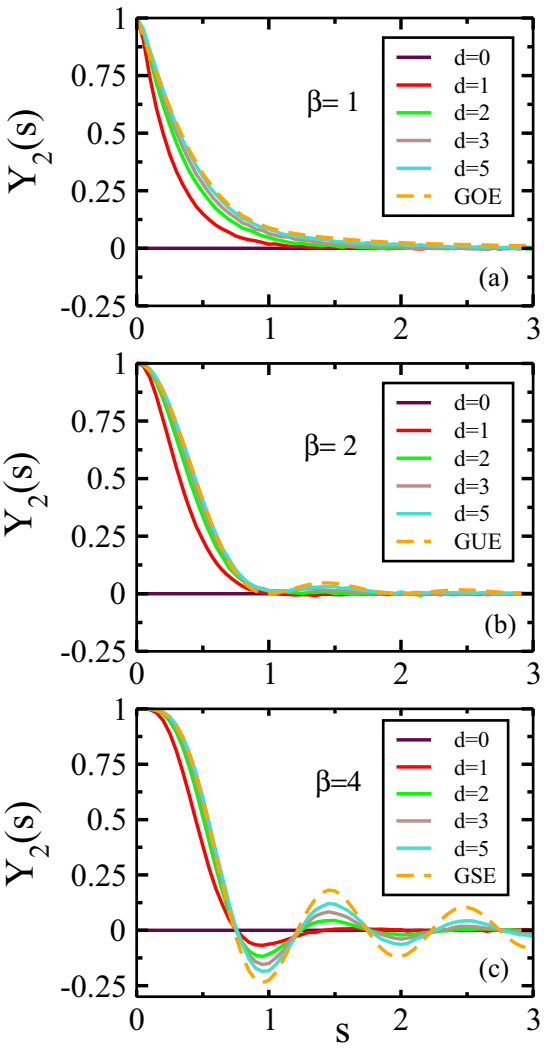

FIG. 6. Analogous to Fig. 5, but for the two-point cluster function: $Y_2(s) = 1 - R_2(s)$.

U_{mn} in Eq. (12). For the weakly chaotic regime (small α), we consider a single matrix of large size. For the strongly chaotic regime (large α), we study an ensemble of matrices generated for values of α in a small window around an average $\bar{\alpha}$. In the latter case, we will label the results by the value of $\bar{\alpha}$.

B. Banded random matrices

Next, we introduce BRM ensembles $\{A\}$ of dimensionality N. The matrix A is banded if $A_{jk} = 0$ for $|j - k| > b$, where b is the bandwidth. The JPD of the matrix distribution for Gaussian BRM ensembles is

$$P(A) = C \exp(-\mathrm{Tr}A^2/4v^2), \tag{13}$$

with v^2 being the variance of the nonzero off-diagonal matrix elements. The matrices A can be real symmetric, complex Hermitian, or quaternion self-dual corresponding to $\beta = 1, 2, 4$ respectively. For $b = N - 1$, the GOE, GUE, and Gaussian symplectic ensemble are recovered, respectively. We can also generalize Eq. (13) to the non-Gaussian case, where A^2 in the exponent is replaced by a positive-definite function of A. We will not discuss the non-Gaussian case here.

It can be shown that the eigenvalue density of the BRM is semicircular, as in the classical ensembles [32]. The density is given by

$$\rho(x) = \frac{2\sqrt{R^2 - x^2}}{\pi R^2}, \tag{14}$$

where the radius $R^2 = 8\beta b v^2$. However, the number of eigenvalues outside the semicircle increases as b decreases. For example, for $N = 1001$ the number of eigenvalues outside the semicircle is 1–2 for the classical case, as compared to 10–20 for the BRM with $b \simeq 50$.

There have been several important studies of the level statistics of BRMs. Fyodorov and Merlin [33] have studied BRMs analytically using the supersymmetric nonlinear sigma model. They demonstrated that this model exhibits localization on the scale $\ell \sim b^2$. They also showed that the

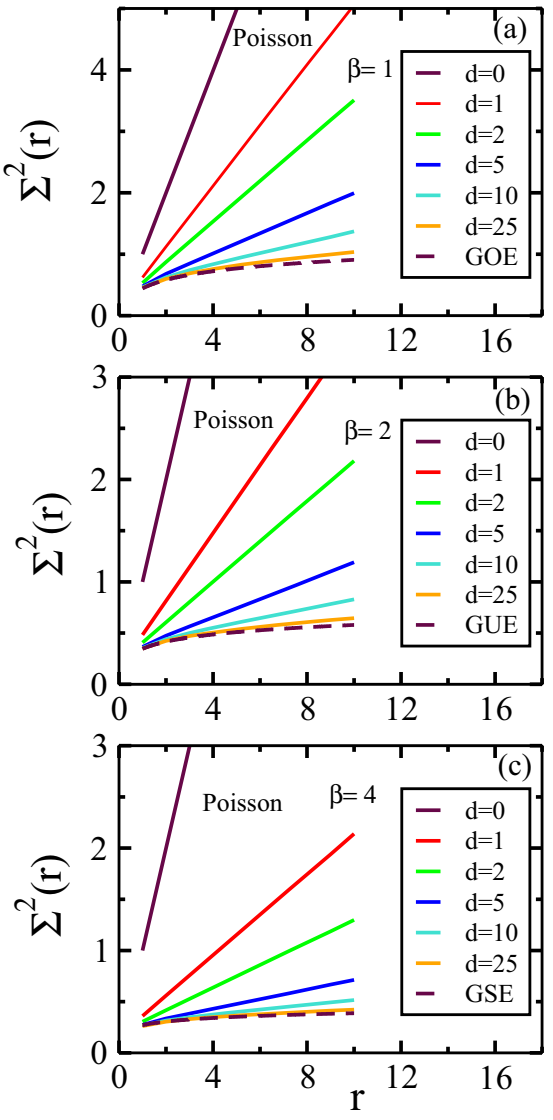

FIG. 7. Number variance $[\Sigma^2(r)$ vs $r]$ for FRCG models with $d = 0, 1, 2, 5, 10, 25$. We show results for (a) $\beta = 1$, (b) $\beta = 2$, and (c) $\beta = 4$. The dashed line denotes the classical Gaussian ensemble result.

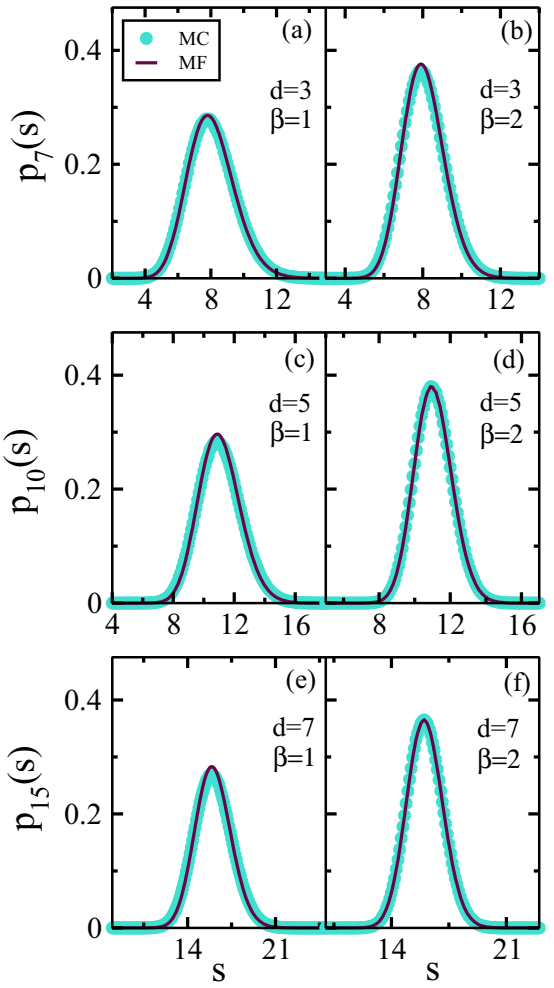

FIG. 8. Spacing density $[p_{n-1}(s)$ vs $s]$ for FRCG models. We consider various values of d, β, and n as indicated. The filled circles correspond to MC results, and the solid lines denote the MF result from Eq. (91) of Ref. [13].

nonlinear sigma model was equivalent to a one-dimensional disordered wire with diffusion constant $D \sim \ell$. Numerical experiments by Casati *et al.* [34,35] confirmed the localization of eigenvectors of BRMs on the scale ℓ. Casati *et al.* [36] also showed a similar localization of eigenvectors in random matrices of quantum chaotic systems.

Fyodorov and Mirlin [33] also proposed that the BRM ensemble with bandwidth range $1 \to N - 1$ is suitable for interpolating between the integrable regime (with Poisson statistics) and the chaotic regime (with classical RMT statistics) of time-reversal invariant quantum systems. We discuss these limits in the context of the diffusion constant D. The dynamics is diffusive in the limit $D/N = b^2/N \gg 1$. In this case, Altshuler and Shklovskii [37] have showed that the spectral statistics obey classical RMT. In the opposite limit $b^2/N \ll 1$, the dynamics is localized and we expect Poisson statistics to apply.

C. Connection between QKR, BRM, and FRCG models

It has empirically been shown by several authors [29,34–36] that BRMs and QKRs give the same nearest-neighbor spacing density $p_0(s)$ when $b^2/N = \alpha^2/N$. These authors also showed that, in the momentum representation, the QKR matrix U is banded.

Let us examine the structure of operators in the QKR evolution. We will first demonstrate that, even though p and $\cos\theta$ are nonrandom operators, they have matrix properties analogous to Gaussian random matrix ensembles in U-diagonal representation. The randomness arises from the statistical properties of eigenvectors of $U(\alpha)$, which are similar to those of Gaussian ensembles.

We first consider the case with $\gamma = 0$. The $\cos\theta$ operator in U-diagonal representation has matrix properties analogous to the GOE (not shown here). However, since its eigenvalues are fixed, there are weak correlations among different matrix elements. Similarly, when we write p in U-diagonal representation, it has matrix properties analogous to a Gaussian BRM ensemble with width depending on α. The matrix elements

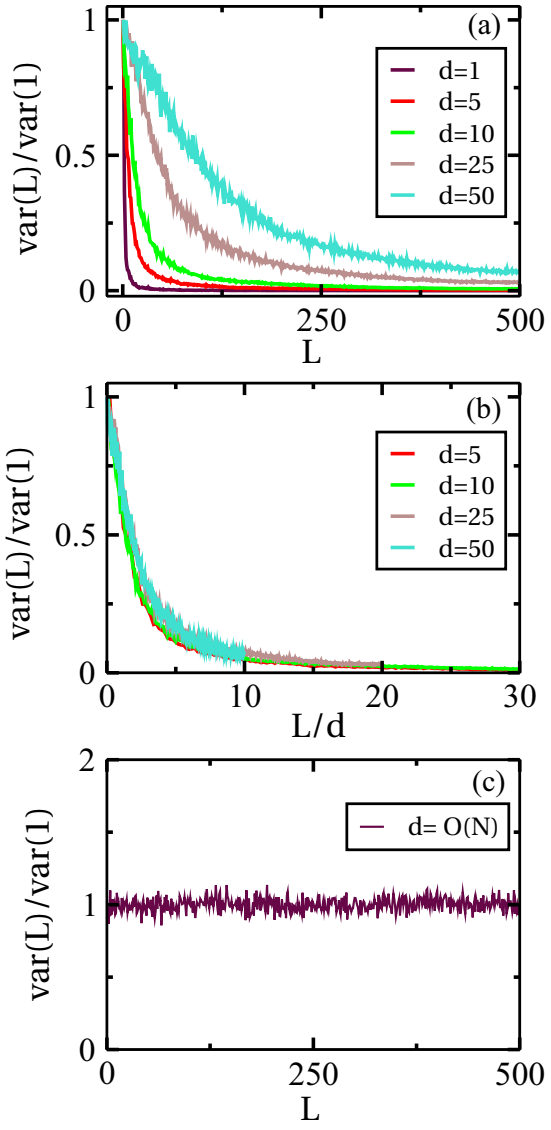

FIG. 9. (a) Plot of var(L)/var(1) vs L for the QKR momentum operator in the U-diagonal basis. We have $\gamma = 0$, and the values of α are such that $d = \alpha^2/N = 1, 5, 10, 25, 50$. (b) Data in panel (a), plotted against the scaled variable L/d. (c) Analogous to panel (a), but for a large value of α so that $d = O(N)$.

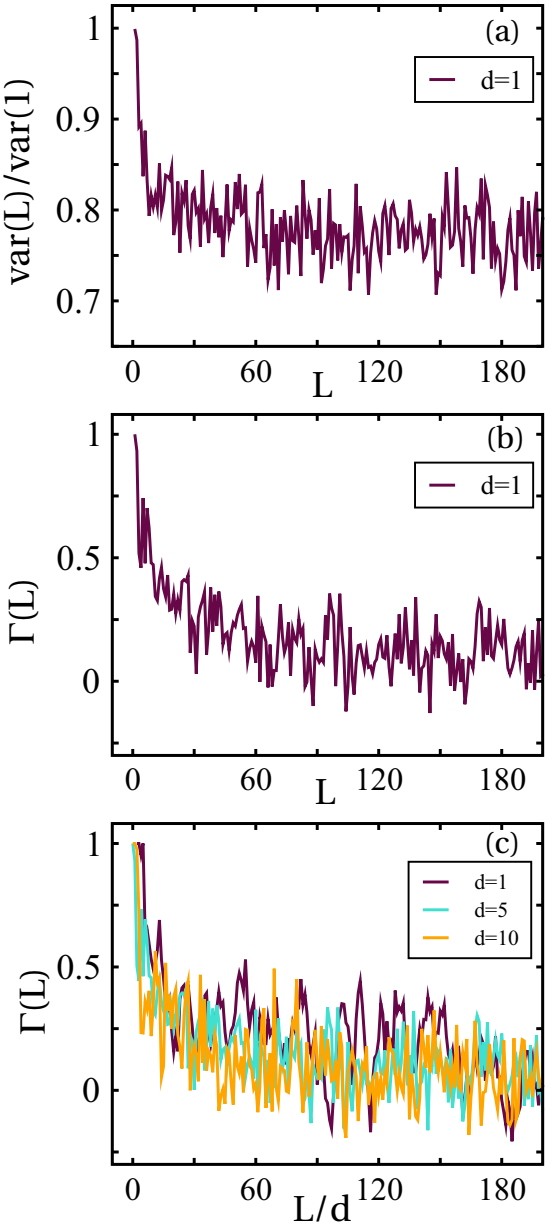

FIG. 10. (a) Plot of var(L)/var(1) vs L for the BRM. The bandwidth $b = 32$, so that $d = b^2/N = 1$. (b) Plot of $\Gamma(L)$ vs L for the data in panel (a). (c) Superposition of $\Gamma(L)$ vs L/d for $b = 32, 72, 100$ so that $d = 1, 5, 10$.

p_{jk} in the position basis of U are given by

$$p_{jk} \equiv \langle \phi_j | p | \phi_k \rangle = \sum_{m,n} \langle \phi_j | m \rangle \langle m | p | n \rangle \langle n | \phi_k \rangle. \quad (15)$$

Here, $|\phi_j\rangle$ represents the eigenfunctions of the evolution operator U, and $|m\rangle$ represents the basis of the momentum operator. Note that p is a diagonal matrix in the self-basis. Equation (15) can be simplified to

$$p_{jk} = \frac{1}{N} \sum_{l,m,n} l\hbar\, e^{i2\pi l(m-n)/N} \langle \phi_j | m \rangle \langle n | \phi_k \rangle, \quad (16)$$

where the eigenfunctions are ordered by the corresponding eigenvalues. At this stage, it is useful to introduce the parameter $d = \alpha^2/N$, which will shortly be identified as the range of the corresponding FRCG model. Let us first consider some values of α for which $d \ll N$. In Fig. 9(a), we plot the normalized variance of the off-diagonal elements of p, var(L)/var(1) vs L, where L is the distance from the diagonal. We see that the variance decays rapidly with L, demonstrating that p is banded. A very interesting property of var(L) is that the decay rate scales linearly with d. This is shown in Fig. 9(b), where var(L)/var(1) is plotted against L/d, resulting in a neat data collapse. Figure 9(c) shows the corresponding plot for $\alpha = 1000$ so that $d = O(N)$. In this case, the p matrix is no longer banded. For large d, the variance is var(L) $\simeq N/12$ [31].

For $\gamma = 0.7$ (which satisfies $\gamma \gg N^{-3/2}$ [31]), the above scenario applies again for the operators $\cos\theta$ and p, with

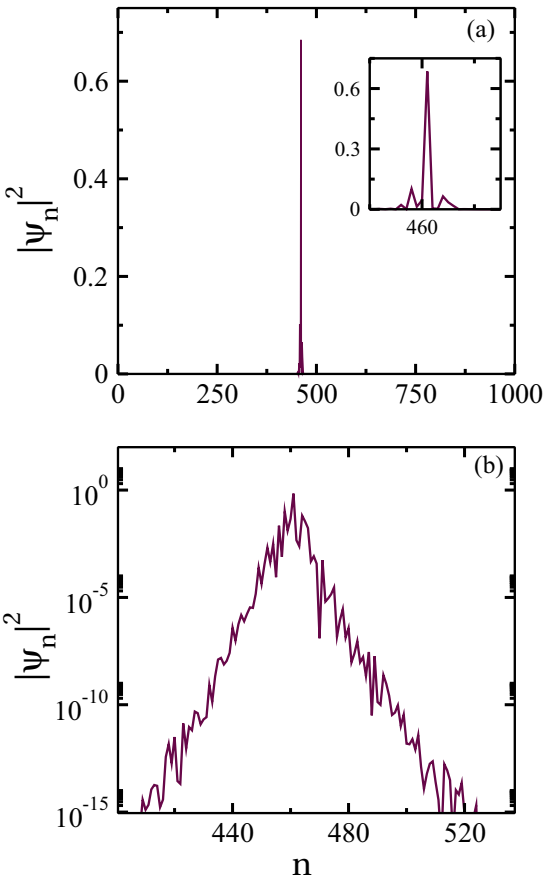

FIG. 11. Typical eigenvector of a BRM with bandwidth $b = 5$. (a) Plot of $|\psi_n|^2$ vs n on a direct scale. Here, n is the component of the eigenvector. The inset shows an expanded region near the point of localization. (b) Data in panel (a), plotted on a linear-log scale. The eigenfunction decays exponentially from the point of localization.

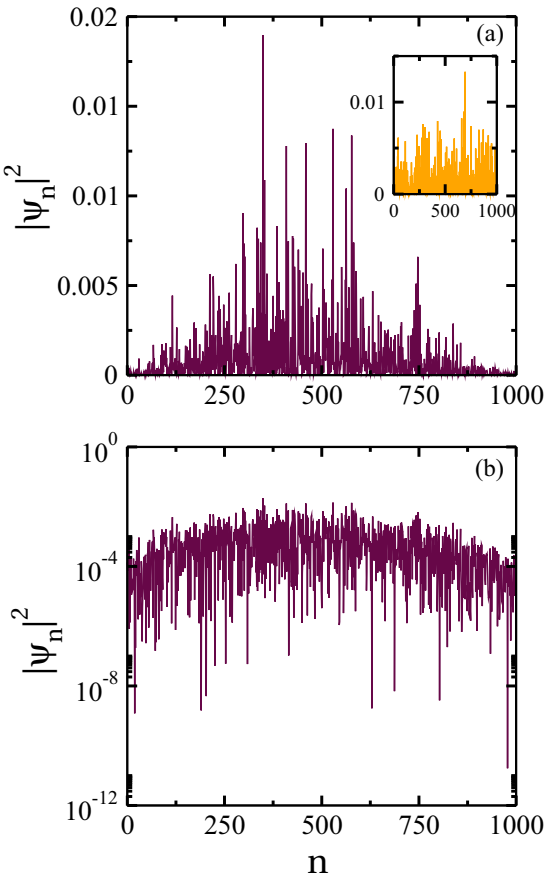

FIG. 12. Typical eigenvector of a BRM with bandwidth $b = 250$ so that $d = 63$. (a) Plot of $|\psi_n|^2$ vs n. This corresponds to an extended state. The inset shows the eigenvector when $d = N - 1$. (b) Data in panel (a), plotted on a linear-log scale.

GOE-like matrices replaced by GUE-like matrices. The p matrices are banded (on a scale $d = \alpha^2/N$) or extended, depending on the value of α.

We have demonstrated above that BRMs arise naturally in the study of QKRs [34–36]. Let us next examine some properties of BRMs. We start with the observation that the sum of two BRMs B_1 and B_2, with the same bandwidths b and variances v_1^2 and v_2^2, is also a BRM of bandwidth b with variance $v_1^2 + v_2^2$. The indices 1 and 2 in B_1 and B_2 refer to two independent BRMs, which have similar structures in all respects. We investigate the statistics of the matrix elements of B_2 in the B_1-diagonal representation. For simplicity, we consider the case with $\beta = 1$. The cases $\beta = 2, 4$ yield similar results.

In Fig. 10(a), we plot the variance of $B_{2,jk}$ as a function of $L = |j - k|$. The bandwidth $b = 32$, so that $d = b^2/N = 1$. We observe that the variance decays rapidly as in Fig. 9(a), but settles to a nonzero value K. This constant is approximately $\mathrm{Tr}B_2^2/N^2$ for large N, and arises due to the semicircular level density of B_2, as specified in Eq. (14). The constant K is roughly equal to the radius R of this semicircle. Thus, for different bandwidth b (and hence different d), we have distinct values of K. If we substract this constant from the respective variances, the modified variances $\Gamma(L)$ decay and saturate to zero. In Fig. 10(b), we plot

$$\Gamma(L) = \frac{\mathrm{var}(L) - K}{\mathrm{var}(1) - K} \tag{17}$$

as a function of L for the data in Fig. 10(a). The decay rate is again proportional to d, which is confirmed by plotting $\Gamma(L)$ vs L/d for $d = 1, 5, 10$ in Fig. 10(c).

Next we turn our attention to the structure of eigenvectors of BRMs. In Fig. 11(a), we plot $|\psi_n|^2$ vs n, where ψ_n is the component of a typical eigenvector of B_2 with $b = 5$. It is sharply localized around a particular value of n. In Fig. 11(b), we plot $|\psi_n|^2$ vs n on a linear-log scale. This plot shows that the decay of eigenvectors is exponential in the distance from the peak. This localization disappears as d increases. In Fig. 12, we plot a typical $|\psi_n|^2$ vs n for $b = 250$, and see that the eigenvector is extended.

Where do FRCG models fit into the above framework? We have proposed recently [23] that QKRs and BRMs can be modeled by FRCG with range

$$d = \alpha^2/N = b^2/N, \tag{18}$$

valid for all fluctuation measures. As we will see shortly, both the diffusive and localized limits discussed in Sec. IV B

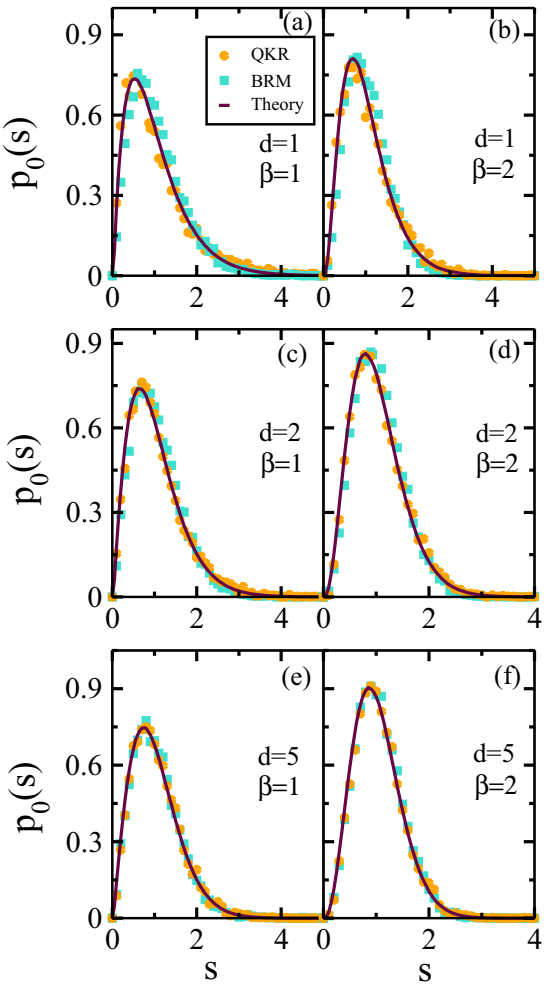

FIG. 13. Spacing density $p_0(s)$ vs s for the QKR and BRM. The solid line denotes the FRCG result. We show data for various values of d and β, as indicated.

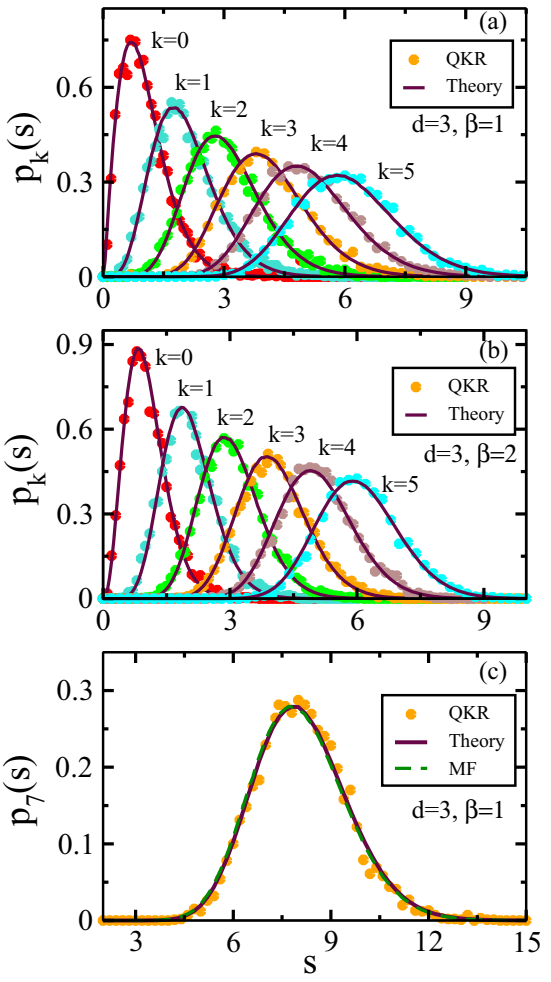

FIG. 14. Spacing density $p_{n-1=k}(s)$ vs s for the QKR. The solid line denotes the FRCG result. (a) Data for $d = 3, \beta = 1$ with $k = 0, 1, 2, 3, 4, 5$. (b) Data for $d = 3, \beta = 2$ with $k = 0, 1, 2, 3, 4, 5$. (c) Data for $d = 3, \beta = 1$ with $k = 7$. We also superpose the MF result.

are realized in our FRCG models. We should emphasize that the range d, as defined in Eq. (18), can also take noninteger values. Therefore, we will subsequently introduce FRCG models with fractional values of d. This will facilitate a better understanding of the Poisson–Wigner-Dyson crossover as d goes from zero to $N - 1$.

V. SPECTRAL FLUCTUATIONS FOR QKR AND BRM MODELS AND COMPARISON WITH FRCG MODELS

In this section, we present a detailed comparison between our FRCG results (obtained by analytic and MC approaches) and numerical results for QKRs and BRMs. In our subsequent discussion, the term "theory" will refer to the FRCG results. For the QKR, we consider the matrices U_{nm}. For the BRM, we study banded matrices with elements of the GOE type or GUE type. It is useful to summarize here various parameters for our numerical studies. The numerical results for QKRs shown below correspond to $N = 1001$ (unless otherwise stated), $\theta_0 = \pi/2N$, and $\gamma = 0.0$ and 0.7. We will show results for several values of the kicking parameter α. Our numerical results for BRMs correspond to $N = 1001$, and several values of the bandwidth b.

Before presenting results for spectral fluctuations, it is important to clarify a technical detail about the procedure we adopt for unfolding of the eigenvalue spectrum. For the QKR, the level density of eigenvalues is uniform. Therefore, a multiplication factor of $N/2\pi$ makes the average density unity everywhere. As mentioned in Sec. IV, BRMs have the additional feature that the level density is semicircular. In this case, for unfolding purposes, we use the radius given after Eq. (14).

In Fig. 13, we show results for $p_0(s)$ vs s for QKRs and BRMs. In Fig. 14, we plot the higher-order spacing distribution $p_k(s)$ for $d = 3$ and $\beta = 1, 2$ in QKRs. In both figures, the agreement between QKR and BRM results and FRCG results is excellent. In Fig. 14(c), we have also plotted the MF result from Sec. IX of Ref. [13]. Note that the results for $d = 0, 1, 2$ are obtained analytically in Ref. [13]. The FRCG results for $d = 3, 5$ are obtained via the MC technique.

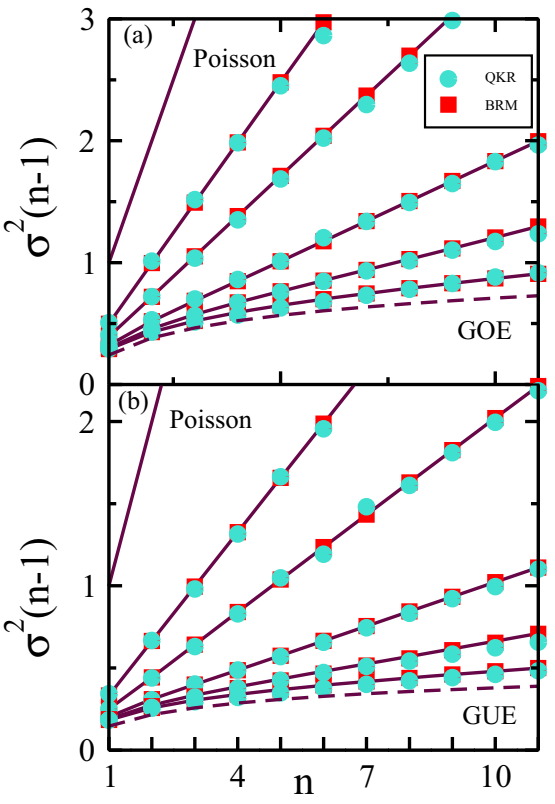

FIG. 15. Spacing variance $\sigma^2(n-1)$ vs n for the QKR and BRM. We show data for $d = 0, 1, 2, 5, 10, 25, N-1$ (from top to bottom), and (a) $\beta = 1$ and (b) $\beta = 2$. The solid lines denote the corresponding FRCG results. The dashed lines denote the classical ensemble results.

In Fig. 15, we show the spacing variance for $\sigma^2(n-1)$ vs n for QKRs and BRMs with $N = 5001$. We have considered several values of d in both the GOE and GUE. As before, we compare our QKR and BRM results with theory from FRCG models, and see that the agreement is excellent. We make the following observations.

(a) $\sigma^2(n)$ vs n is linear for both GOE and GUE for $d = O(1)$. For $d = O(N)$, $\sigma^2(n)$ shows logarithmic behavior as in classical statistics.

(b) The spacing variance in the $\beta = 2$ case is roughly half of that in the $\beta = 1$ case for each value of n.

These behaviors are qualitatively similar to our analytical results for FRCG models in Ref. [13].

In Figs. 16 and 17, we plot $R_2(s)$ vs s for QKRs with $\beta = 1, 2$, and compare with FRCG results. Again, there is very good agreement between QKRs and theory. For comparison, we plot $R_2(s)$ vs s in Figs. 18 and 19 for BRMs. Notice that our results are already very close to the relevant classical result (GOE or GUE) for $d = 3$. Thus, there is a rapid transition from Poisson ($d = 0$) to classical ($d = N-1$) results.

A more quantitative comparison with physical systems may require the introduction of Coulomb gas models where the interaction strength decays gradually with distance rather than the sharp cutoff considered here. This will be part of our future investigation of this problem.

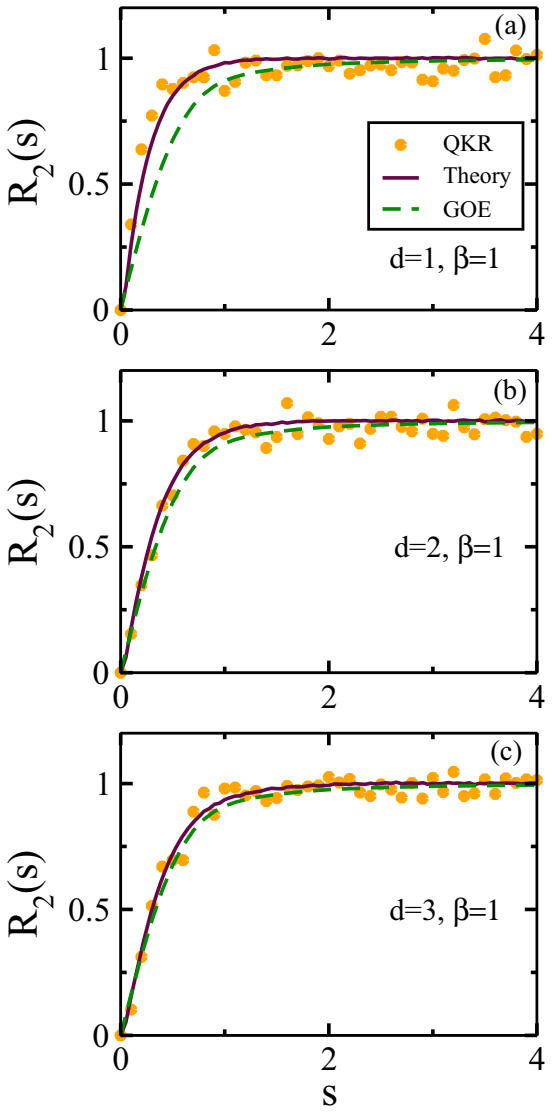

FIG. 16. Two-point correlation function $R_2(s)$ vs s for the QKR. The solid lines denote the corresponding FRCG results. The dashed lines denote the GOE result. We show data for $\beta = 1$ and (a) $d = 1$, (b) $d = 2$, and (c) $d = 3$.

VI. FRACTIONAL VALUES OF D: COMPARISON WITH THE QKR MODEL

Our discussion so far has focused on integer values of d. However, the parameter d relevant for QKRs ($d = \alpha^2/N$) and BRMs ($d = b^2/N$) can take noninteger values also. For a complete description of QKRs and BRMs with arbitrary d, we introduce an FRCG model with fractional d. We generalize the JPD for nearest-neighbor spacings in Sec. VII of Ref. [13] as follows:

$$P_d(s_1, \ldots, s_N) = C_d \delta\left(\sum_{i=1}^{N} s_i - N\right) \prod_{j=1}^{N} \prod_{k=0}^{[d]} (s_j + \ldots + s_{j+k})^{\beta\Delta(k)}, \quad (19)$$

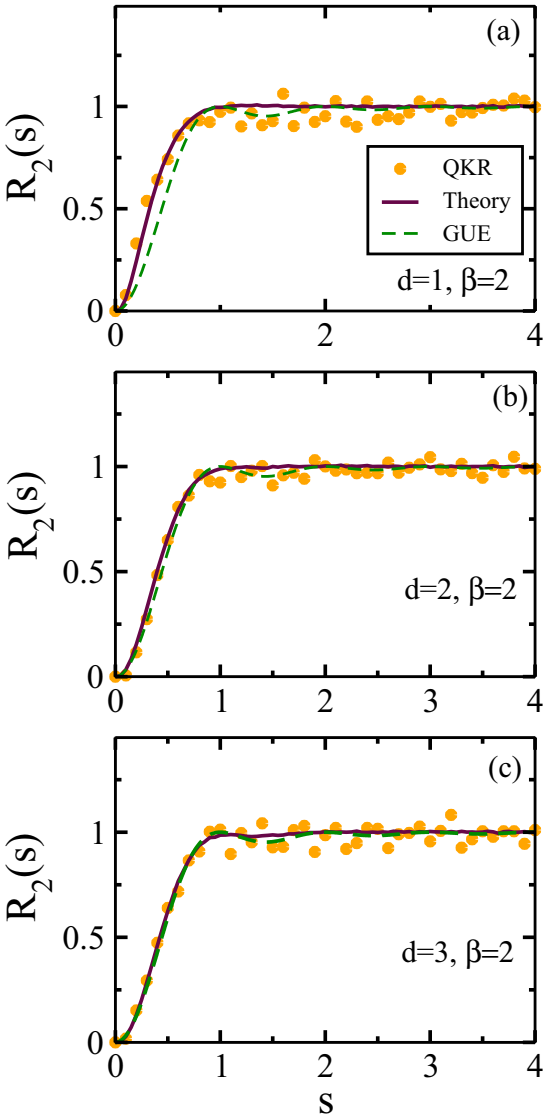

FIG. 17. Analogous to Fig. 16, but for the $\beta = 2$ case.

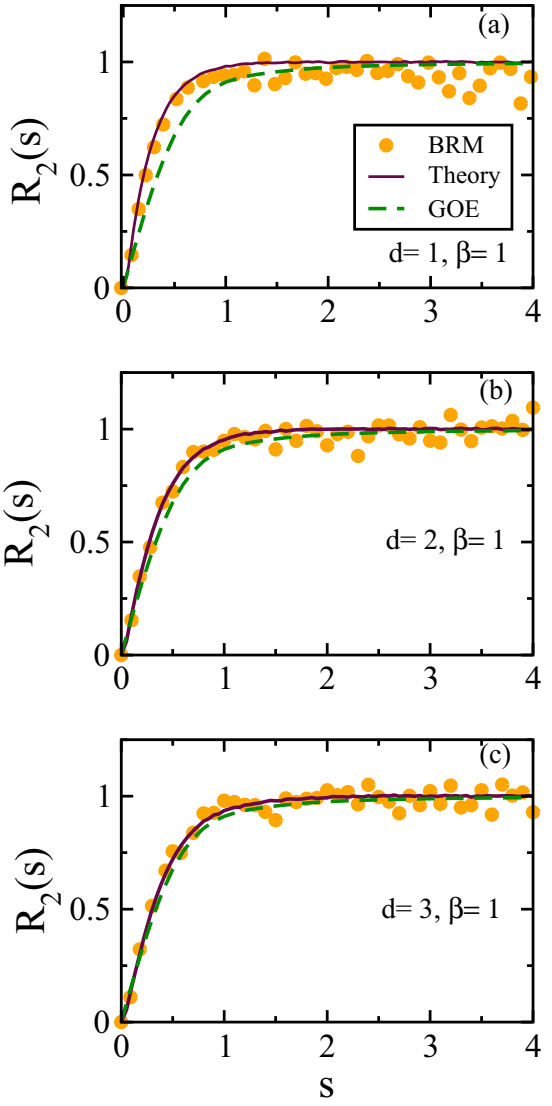

FIG. 18. Two-point correlation function $R_2(s)$ vs s for the BRM. The solid lines denote the corresponding FRCG results. The dashed lines denote the GOE result. We show data for $\beta = 1$ and (a) $d = 1$, (b) $d = 2$, and (c) $d = 3$.

where $[d]$ is the largest integer $\leqslant d$. Moreover, $\Delta(k) = 1$ for $k = 0, 1, \ldots, [d] - 1$, and $\Delta([d]) = d - [d]$. We make the following observations.

(i) For integer d, Eq. (19) reduces to the definition of P_d in Eq. (56) of Ref. [13].

(ii) All cases with $0 \leqslant d \leqslant 1$ are analytically tractable as there are only one-particle terms in P_d. This case is analogous to the $d = 0, 1$ cases in Sec. VIII of Ref. [13]. The corresponding nearest-neighbor distribution is

$$p_0(s) = \frac{(\beta d + 1)^{(\beta d+1)}}{\Gamma(\beta d + 1)} s^{\beta d} e^{-(\beta d+1)s}. \tag{20}$$

The $(n-1)$th spacing distribution is given by

$$p_{n-1}(s) = \frac{(\beta d + 1)^{(\beta d+1)n}}{\Gamma[(\beta d + 1)n]} s^{(\beta d+1)n-1} e^{-(\beta d+1)s}. \tag{21}$$

(iii) Our choice of $\Delta(k)$ ensures that the MF approximation of P_d yields the results in Eqs. (20) and (21) even for noninteger d.

Next, we present some results for noninteger d in Fig. 20. The theoretical results are obtained via MC in this case. We plot $p_0(s)$ vs s for QKR and FRCG models with $d = 1.5, 2.5, 3.5$ and $\beta = 1, 2$. The excellent agreement confirms the applicability of our fractional FRCG model to understand the spectral statistics of QKRs.

VII. SUMMARY AND DISCUSSION

Let us conclude this paper with a summary and discussion of our results in this two-part exposition on FRCG models and their application in physical systems.

In Ref. [13], we introduced FRCG models as a natural generalization of Dyson's Brownian motion models for eigenvalue spectra of random matrix ensembles. These are

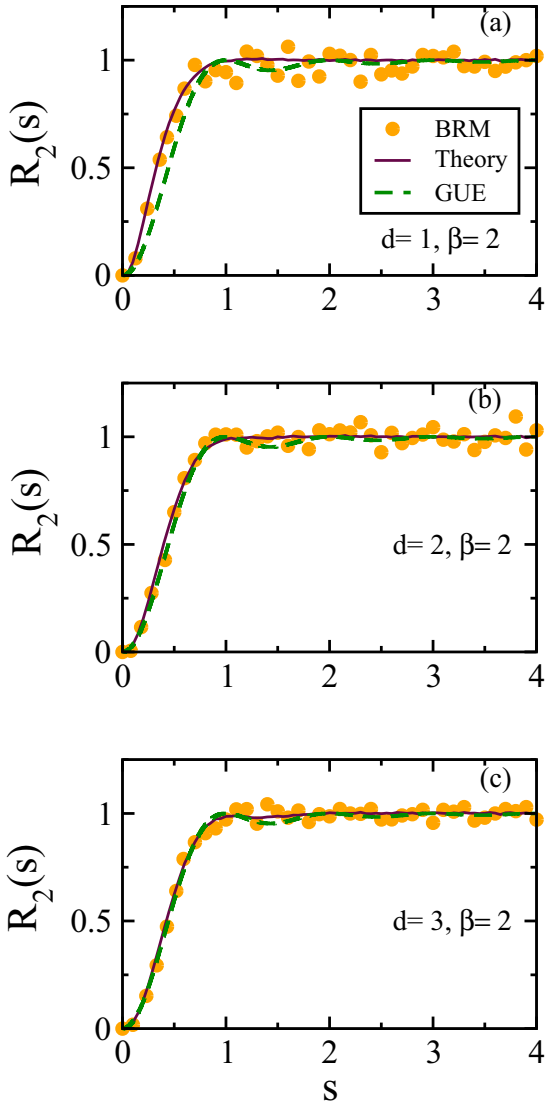

FIG. 19. Analogous to Fig. 18, but for the $\beta = 2$ case.

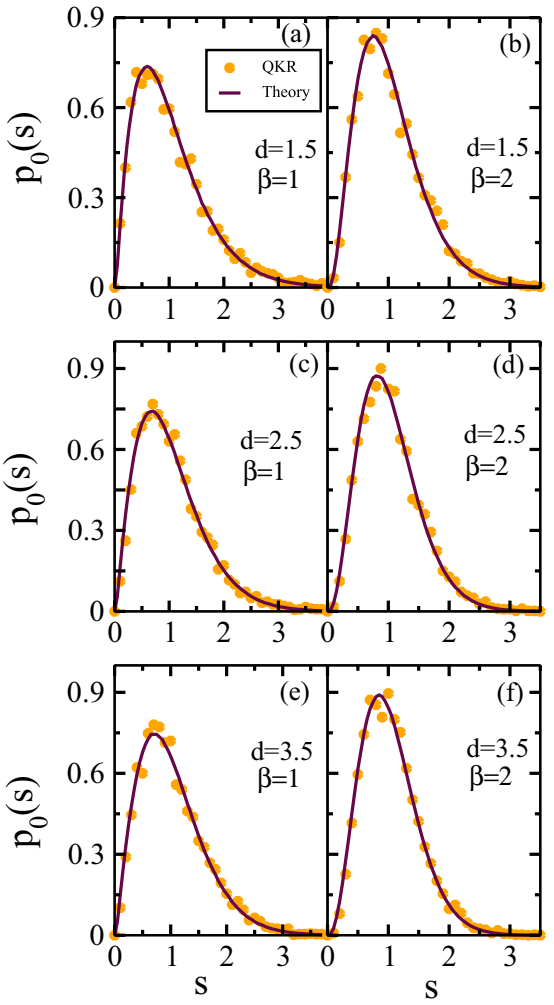

FIG. 20. Plot of $p_0(s)$ vs s for the QKR with fractional values of d. The solid lines denote the appropriate FRCG result. We show results for various values of β and d, as indicated.

parametrized by the range of interactions between eigenvalues, denoted as d. Our FRCG models provide a route for transition from Poisson statistics (for $d = 0$) to classical random matrix statistics (for $d = N - 1$, where N is the dimensionality of the matrices). In Ref. [13], we also introduced an integral-equation approach for analytical solution of these FRCG models. The integral equation is analytically tractable for $d \leqslant 2$. However, for $d > 2$, the equations become increasingly complicated. For $d > 2$, we have proposed a MF approximation, which yields simple and accurate solutions. In this paper (part II in the series), we have also proposed a MC technique which yields precise results for spectral statistics of FRCG models. The MC technique is validated by comparison with analytical results, wherever these are available. We use the term "theory" to describe exact analytic and MC results for FRCG models.

It is natural to ask whether the elegant framework of FRCG models has useful physical applications. This is the primary focus of the present paper, where we have demonstrated that the eigenvalue statistics of QKRs and BRMs is described by FRCG models. The QKRs are characterized by a kicking parameter α, which describes how chaotic the system is. The BRMs are parametrized by the bandwidth b, which is the off-diagonal distance up to which the matrix has nonzero entries. Earlier work has shown that QKRs and BRMs yield the same results for $p_0(s)$ if $\alpha^2/N = b^2/N$. In this paper, we have shown that FRCG models with $d = \alpha^2/N = b^2/N$ provide a framework for deriving the spectral properties of QKRs and BRMs. We have presented results from a detailed comparison of diverse spectral properties in QKRs, BRMs, and FRCG. In all cases, the agreement is excellent.

The QKR has been a fundamental paradigm in the area of quantum chaos. Therefore, it is gratifying to see that FRCG models provide an excellent description of the QKR statistics. An important direction for future research is the identification of other physical systems which are modeled by FRCG. There are many systems which exhibit a crossover from Poisson to classical statistics as a parameter is varied. In this context, there have been studies of diverse systems such as atomic spectra [38], random matrix models [39], quantum chaotic systems [40,41], Anderson localization [19,42,43],

quark-gluon plasma [44], and neural networks [45]. Clearly, there are several different routes whereby this transition can be realized. It is our belief that the FRCG scenario may find application in several of these systems.

ACKNOWLEDGMENT

S.P. is grateful to the Department of Science and Technology (India) for support through a J.C. Bose fellowship.

[1] M. L. Mehta, *Random Matrices* (Academic, New York, 2004).
[2] T. A. Brody, J. Flores, J. B. French, P. A. Mello, A. Pandey, and S. S. M. Wong, Rev. Mod. Phys. **53**, 385 (1981).
[3] *Statistical Theories of Spectra: Fluctuations*, edited by C. E. Porter (Academic, New York, 1965).
[4] E. P. Wigner, SIAM Rev. **9**, 1 (1967).
[5] O. Bohigas and M. J. Giannoni, *Chaotic Motion and Random Matrix Theories* (World Scientific, Singapore, 1985).
[6] O. Bohigas, M. J. Giannoni, and C. Schmit, Phys. Rev. Lett. **52**, 1 (1984).
[7] G. Casati and B. Chirikov, *Quantum Chaos: Between Order and Disorder* (Cambridge University, Cambridge, England, 1995).
[8] F. Haake, *Quantum Signatures of Chaos* (Springer-Verlag, Heidelberg, 2001).
[9] R. Blumel and W. P. Reinhardt, *Chaos in Atomic Physics* (Cambridge University, Cambridge, England, 2005).
[10] H. Stockmann, *Quantum Chaos: An Introduction* (Cambridge University, Cambridge, England, 2006).
[11] T. H. Seligman, J. J. M. Verbaarschot, and M. R. Zirnbauer, Phys. Rev. Lett. **53**, 215 (1984); T. Cheon, *ibid.* **65**, 529 (1990).
[12] T. H. Seligman and J. J. M. Verbaarschot, in *Proceedings of the Fourth International Conference on Quantum Chaos and the 2nd Colloquium on Statistical Nuclear Physics*, edited by T. H. Seligman and H. Nishioka (Springer-Verlag, Berlin, 1986), p. 131; C. E. Roman, T. H. Seligman and J. J. M. Verbaarschot, *ibid.*, p. 256.
[13] A. Pandey, A. Kumar, and S. Puri, preceding paper, Phys. Rev. E **101**, 022217 (2020).
[14] E. B. Bogomolny, U. Gerland, and C. Schmit, Phys. Rev. E **59**, R1315(R) (1999).
[15] E. Bogomolny, U. Gerland, and C. Schmit, Eur. Phys. J. B **19**, 121 (2001).
[16] G. Casati, B. V. Chirikov, F. M. Izraelev, and J. Ford, in *Stochastic Behavior in Classical and Quantum Hamiltonian Systems*, edited by G. Casati and J. Ford, Lecture Notes in Physics, Vol. 93 (Springer-Verlag, Berlin, Heidelberg, 1979), pp. 334–352.
[17] R. E. Prange and S. Fishman, Phys. Rev. Lett. **63**, 704 (1989).
[18] S. Fishman, D. R. Grempel, and R. E. Prange, Phys. Rev. Lett. **49**, 509 (1982).
[19] M. Serbyn and J. E. Moore, Phys. Rev. B **93**, 041424(R) (2016).
[20] T. Guhr, A. Muller-Groeling, and H. A. Weidenmüller, Phys. Rep. **299**, 189 (1998).
[21] C. W. J. Beenakker, Rev. Mod. Phys. **69**, 731 (1997).
[22] A. D. Mirlin, Phys. Rep. **326**, 259 (2000).
[23] A. Pandey, A. Kumar, and S. Puri, Phys. Rev. E **96**, 052211 (2017).
[24] H. Risken, *The Fokker-Planck Equation: Methods of Solution and Applications* (Springer, New York, 1984).
[25] A. Pandey, Chaos Solitons Fractals **5**, 1275 (1995).
[26] S. Ghosh, A. Pandey, S. Puri, and R. Saha, Phys. Rev. E **67**, 025201(R) (2003).
[27] A. Pandey, S. Puri, and S. Kumar, Phys. Rev. E **71**, 066210 (2005).
[28] F. M. Izrailev, Phys. Rev. Lett. **56**, 541 (1986).
[29] F. M. Izrailev, Phys. Rep. **196**, 299 (1990).
[30] F. J. Dyson, J. Math. Phys. **3**, 1191 (1962).
[31] A. Pandey, R. Ramaswamy, and P. Shukla, Pramana **41**, L75 (1993).
[32] M. Wilkinson, M. Feingold, and D. M. Leitner, J. Phys. A **24**, 175 (1991).
[33] Y. V. Fyodorov and A. D. Mirlin, Phys. Rev. Lett. **67**, 2405 (1991).
[34] G. Casati, L. Molinari, and F. Izrailev, Phys. Rev. Lett. **64**, 1851 (1990).
[35] G. Casati, F. Izraelev, and L. Molinari, J. Phys. A **24**, 4755 (1991).
[36] G. Casati, I. Guarneri, F. Izrailev, and R. Scharf, Phys. Rev. Lett. **64**, 5 (1990).
[37] B. L. Altshuler and B. I. Shklovskii, Zh. Eksp. Teor. Fiz **91**, 220 (1986) [Sov. Phys. JETP **64**, 127 (1986)].
[38] N. Rosenzweig and C. E. Porter, Phys. Rev. **120**, 1698 (1960).
[39] A. Pandey, Ann. Phys. (NY) **134**, 110 (1981).
[40] D. Wintgen and H. Marxer, Phys. Rev. Lett. **60**, 971 (1988).
[41] T. H. Seligman, J. J. M. Verbaarschot, and M. R. Zirnbauer, J. Phys. A: Math. Gen. **18**, 2751 (1985).
[42] F. Bruckmann, T. G. Kovacs, and S. Schierenberg, Phys. Rev. D **84**, 034505 (2011).
[43] K. Muller, B. Mehlig, F. Milde, and M. Schreiber, Phys. Rev. Lett. **78**, 215 (1997).
[44] T. G. Kovacs and F. Pittler, Phys. Rev. Lett. **105**, 192001 (2010).
[45] A. Amir, N. Hatano, and D. R. Nelson, Phys. Rev. E **93**, 042310 (2016).